Electronic Supplementary Material (ESI) for Chemical Communications.

Supporting Information

Spectroscopic identification of interstellar relevant 2-iminoacetaldehyde

Vladimir D. Drabkin, Viktor Paczelt and André K. Eckhardt*

Lehrstuhl für Organische Chemie II, Ruhr-Universität Bochum, 44801 Bochum (Germany); Andre.Eckhardt@rub.de

Table of Contents

Experimental Section

General remarks. NMR spectra were recorded on Bruker AVIII-300, AVIII-400 and DRX-400 spectrometers at 303 K. Chemical shifts (δ) are given in ppm relative to tetramethylsilane (TMS, δ = 0.00 ppm) as the internal standard or to the respective solvent residual peaks (DMSO: δ = 2.50 and 39.53 ppm; D_2O: δ = 4.79 ppm). GC-MS was carried out on an Agilent Technologies 7820 A gas chromatograph connected to an Agilent Technologies 5977B mass selective detector (EI, 70 eV), respectively, equipped with an Agilent J&W fused silica HP-5MS column (30 m × 0.25 mm × 0.25 μm). Conditions: helium carrier gas, 1.2 mL/min constant flow; injector temperature, 250 °C; source temperature, 230 °C; quadrupole temperature, 150 °C. GC oven temperature program: 60 °C isothermal, 2.5 min; 60 – 250 °C, 40 °C/min; 250 °C, 8.75 min.

Matrix isolation studies[1]. All matrix isolation infrared studies were performed on a Sumitomo RDK 408D2 closed-cycle refrigerator cold head powered by a Sumitomo CSW-71 compressor unit. The vacuum shroud was outfitted with transparent KBr windows and the sample holder mounted at the base of the cold head was outfitted with a polished KBr window transparent in the IR measurement range of 4000-500 cm^{-1}. The temperature on the sample holder was measured by a Si diode and could be adjusted by two resistive heating cartridges operated by a Lakeshore 336 temperature controller. All measurements were conducted at 3 K and an oil diffusion pump was employed to obtain a high vacuum of approximately 1 x 10^{-5} mbar at room temperature. The 2-azidoacetaldehyde (**6**) molecule was evaporated from a glass flask at -10 °C and 2-azidoacetaldehyde-*d3* (**6**-*d3*) at room temperature. During evaporation they were co-condensed onto a KBr window at 12 K with a large excess of argon. The flow rate of the noble gas was set to 2.5 sccm with the help of an MKS mass flow controller and typically 1-1.5 mbar Ar min^{-1} was deposited onto the KBr window from a ~2.5 L silylated glass storage bulb over the course of an hour. For LDA water ice experiments deposition temperature was set to 50K. Water vapour flow was controlled by needle valve. Irradiation experiments were performed using an Osram HBO-200W high-pressure mercury lamp in an Oriel housing in combination with a 260–320 nm dichroic mirror or a Newport Model 77250 1/8m monochromator. For irradiation experiments with a wavelength of 254 nm we employed an Oase Vitronic 11 pool lamp (14 Watt). IR spectra were recorded using a Bruker IFS 66v/s spectrometer collecting 50 scans with a standard resolution of 0.5 cm^{-1} in the 4000–400 cm^{-1} region. For the UV/Vis spectroscopic experiments, a different matrix setup was used with the vacuum shroud equipped with quartz windows and a sapphire window attached to the cold head sample holder. The UV/Vis spectra were recorded using a PerkinElemer Lambda 1050 UV/Vis spectrometer. Spectra were recorded in the 190-800 nm range with a resolution of 1 nm and a scan speed of 266.75 nm min^{-1}. In the range of 190-320 nm a deuterium lamp was used as a light source and switched to a halogen lamp for wavelengths above 320 nm. For the combination of HVFP with matrix isolation we employed a homebuilt, water-cooled oven directly connected to the vacuum shroud of the cryostat. The pyrolysis zone consisted of an empty quartz tube (inner diameter 8 mm, length of heating zone 10 cm) resistively heated by a Thermocoax wire. The temperature was controlled by a Ni/CrNi thermocouple. At a distance of approximately 70 mm, all pyrolysis products were condensed on the surface of the matrix window at 12 K. For all experiments we used Ar of 99.999% purity, and for LDA water ice experiments water was degassed several times prior to the experiment.

Quantum chemical calculations. For all geometry optimizations and frequency calculations the Gaussian16 program package was used[2]. The B3LYP[3–5] hybrid functional together with the 6-311++G(2d,2p) basis set[6,7] was employed for all geometry optimizations, infrared frequency calculations and time-dependent DFT[8–10] calculations for predicting vertical electronic excitation energies. Vibrational frequency calculations were used to characterize stationary points, obtain zero-point vibrational energy corrections and calculate harmonic infrared spectra for comparisons with the experiment. Transition states were characterized by exactly one imaginary frequency and analyzed by IRC calculations in forward and reverse direction. The complete basis set (CBS) energies were extrapolated from explicitly computed cc-pVTZ[11–13] and cc-pVQZ[11–13] single point energies utilizing the

built-in extrapolation[14–16] routine in ORCA 5.0.3.[17] Initial conformational studies were performed using Grimme's xtb[18,19] and CREST[20] program packages. All structures were visualized using Chemcraft[21].

Synthesis

***CAUTION*:** Azides are highly energetic compounds with sensitivity towards heat and impact. Although we had no problem in synthesis, proper protective measures (safety glasses, face shield, leather coat, grounded equipment and shoes, Kevlar® gloves, and ear plugs) should be used when undertaking work involving these compounds.

2-azidoacetaldehyde (**6**)

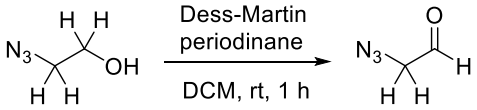

The compound was synthesized according to the procedure of Ii *et. al.*[22] To a solution of 2-azidoethanol (0.32 g, 3.7 mmol) in dichloromethane (DCM) (40 mL) was added Dess-Martin periodinane (2.0 g, 4.7 mmol) dropwise at room temperature and stirred for 1 hour. The solvent was evaporated at 20 °C under reduced pressure and the remaining compound mixture was dissolved in diethyl ether. Insoluble materials were filtered off through a pad of silica/celite. The solvent was removed from the filtrate under reduced pressure at 20 °C and the residue was purified by silica gel column chromatography (3:1, pentane/Et_2O, v/v) to give 2-azidoacetaldehyde (0.2 g, 90%) as a light-yellow oil.

^{1}H NMR (400 MHz, $CDCl_3$): δ = 9.69 (s, 1H, CH), 4.04 (s, 2H, CH_2) ppm.
^{13}C{^{1}H} NMR (76 MHz, $CDCl_3$): δ = 195.1 (CH), 58.8 (CH_2) ppm.

2-azidoacetaldehyde-*d4* (**6-*d4***)

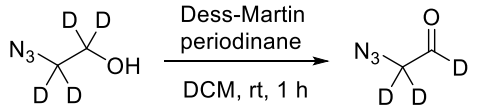

The compound was synthesized in the same fashion using 2-azidoethanol-d_4 (0.32 g, 3.7 mmol) as the starting material.

^{2}H NMR (61 MHz, $CHCl_3$): δ = 9.80 (s, 1D, CD), 4.09 (s, 2D, CD_2) ppm.
^{13}C{^{1}H} NMR (101 MHz, $CDCl_3$): δ = 194.8 (CD), 57.6 (CD_2) ppm.

Infrared and UV/Vis Spectra

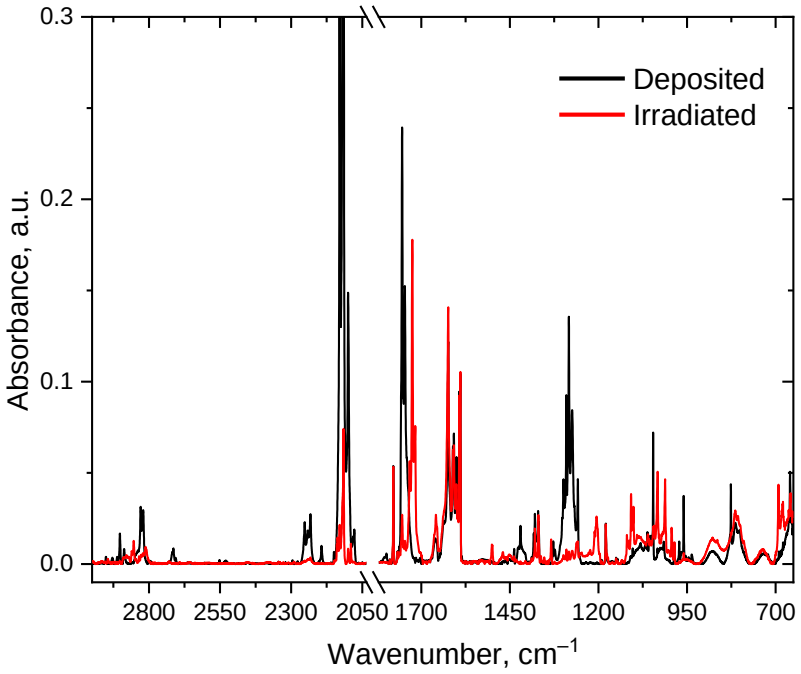

Figure S1. Fragments of FT-IR spectrum of deposited and UV irradiated 2-azidoacetaldehyde (**6**) in solid argon at 3 K.

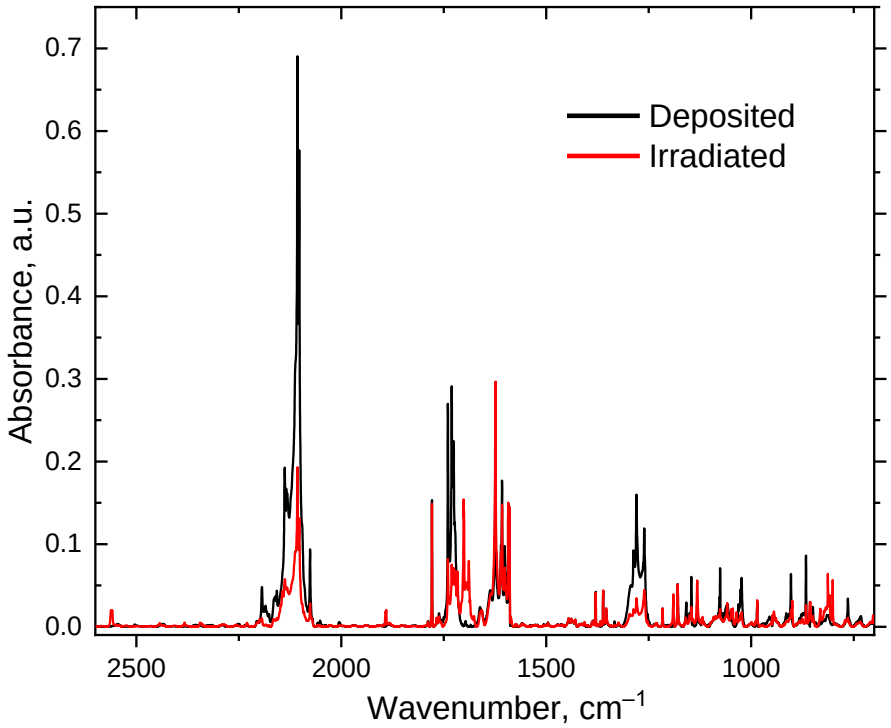

Figure S2. Fragments of FT-IR spectrum of deposited and UV irradiated 2-azidoacetaldehyde-d_3 (**6**-d_3) in solid argon at 3 K.

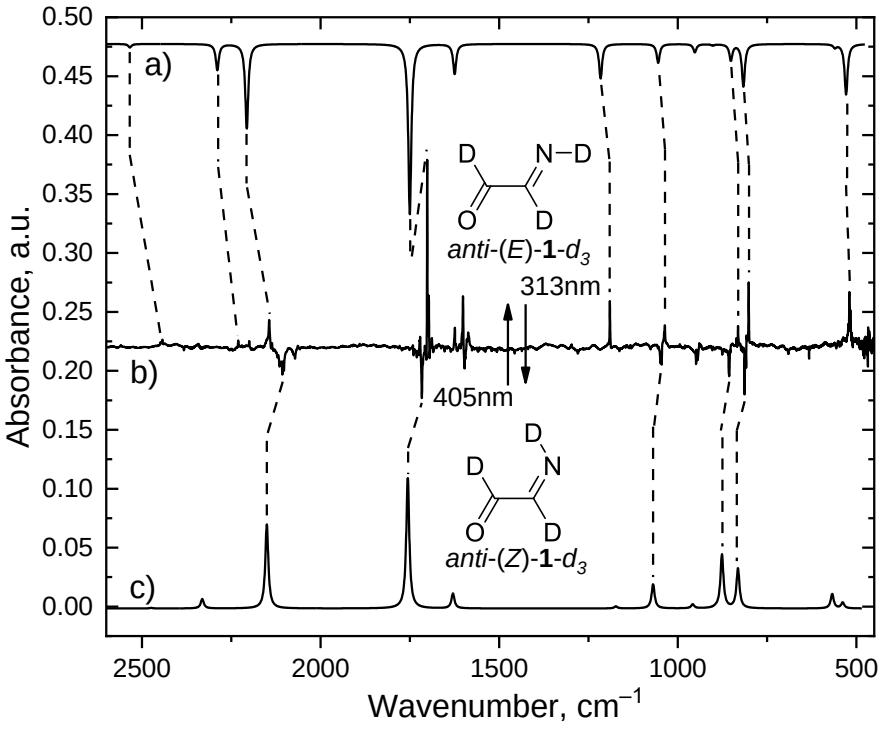

Figure S3. (a and c) Computed harmonic IR spectrum of *anti*-(*E*)-**1**-d_3 and *anti*-(*Z*)-**1**-d_3 at the CCSD(T)/cc-pVTZ level of theory (unscaled); (b) IR difference spectra between the Ar matrix FT-IR spectrum recorded after 45 min photolysis with UV light (λ = 260-320 nm) and 45 min irradiation with λ = 405 nm.

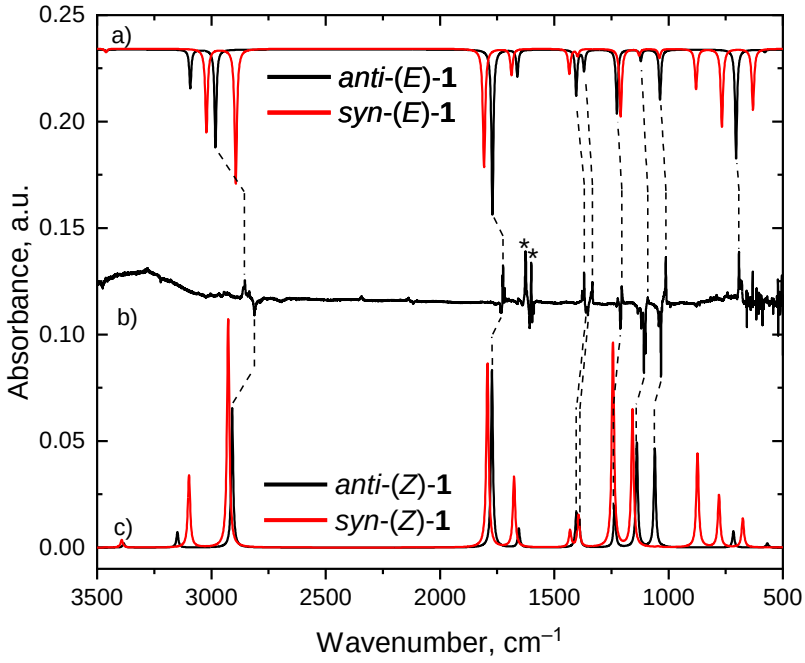

Figure S4. (a) Computed harmonic IR spectrum of *anti*-(*E*)-**1** and *syn*-(*E*)-**1** at the B3LYP/6-311++G(2d,2p) level of theory (unscaled); (c) Computed harmonic IR spectrum of *anti*-(*Z*)-**1** and *syn*-(*Z*)-**1** at the B3LYP/6-311++G(2d,2p) level of theory (unscaled) (b) IR difference spectra between the Ar matrix FT-IR spectrum recorded after 45 min photolysis with UV light (λ = 260-320 nm) and 45 min irradiation with λ = 405 nm.

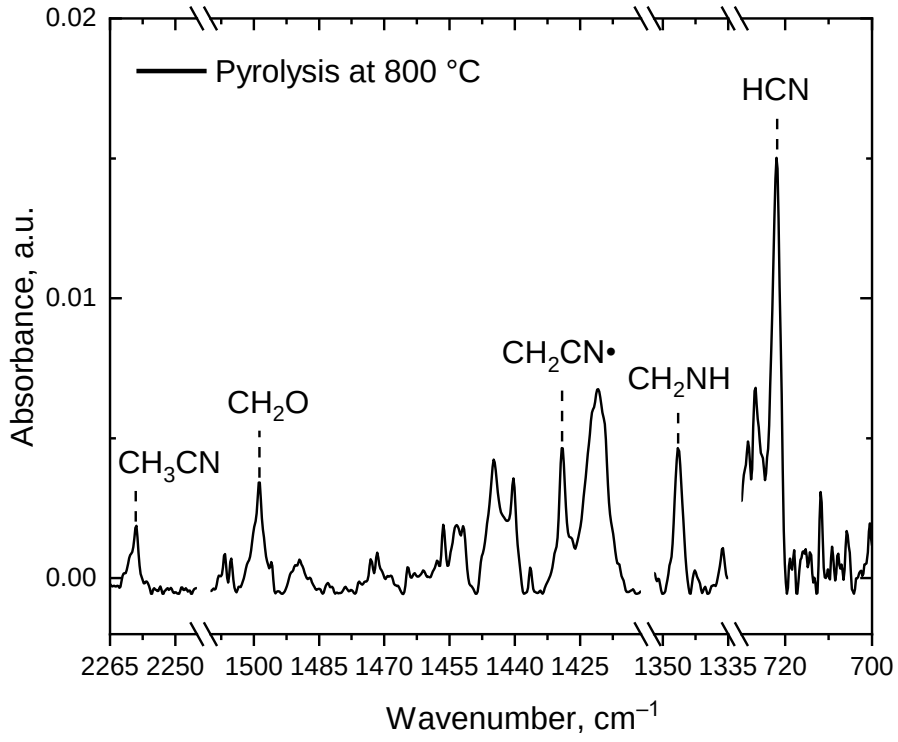

Figure S5. Fragments of the FT-IR pyrolysis spectrum (60 minutes, 800°C) of pyrolyzed 2-azidoacetaldehyde (**6**) in solid argon at 3 K.

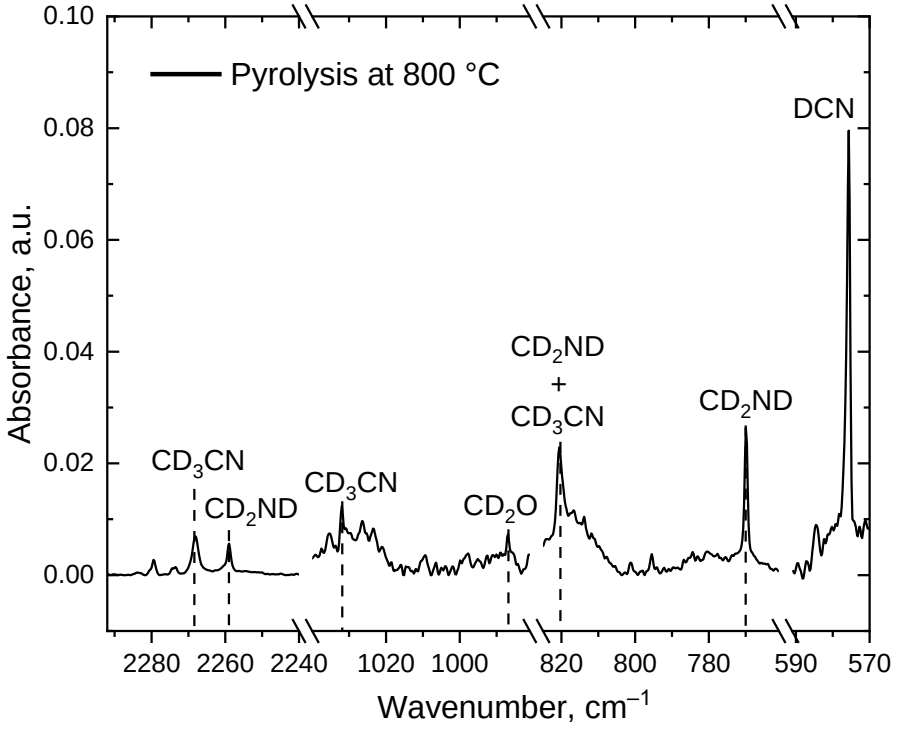

Figure S6. Fragments of the FT-IR pyrolysis spectrum (60 minutes, 800°C) of pyrolyzed 2-azidoacetaldehyde-d_3 (**6**-d_3) in solid argon at 3 K.

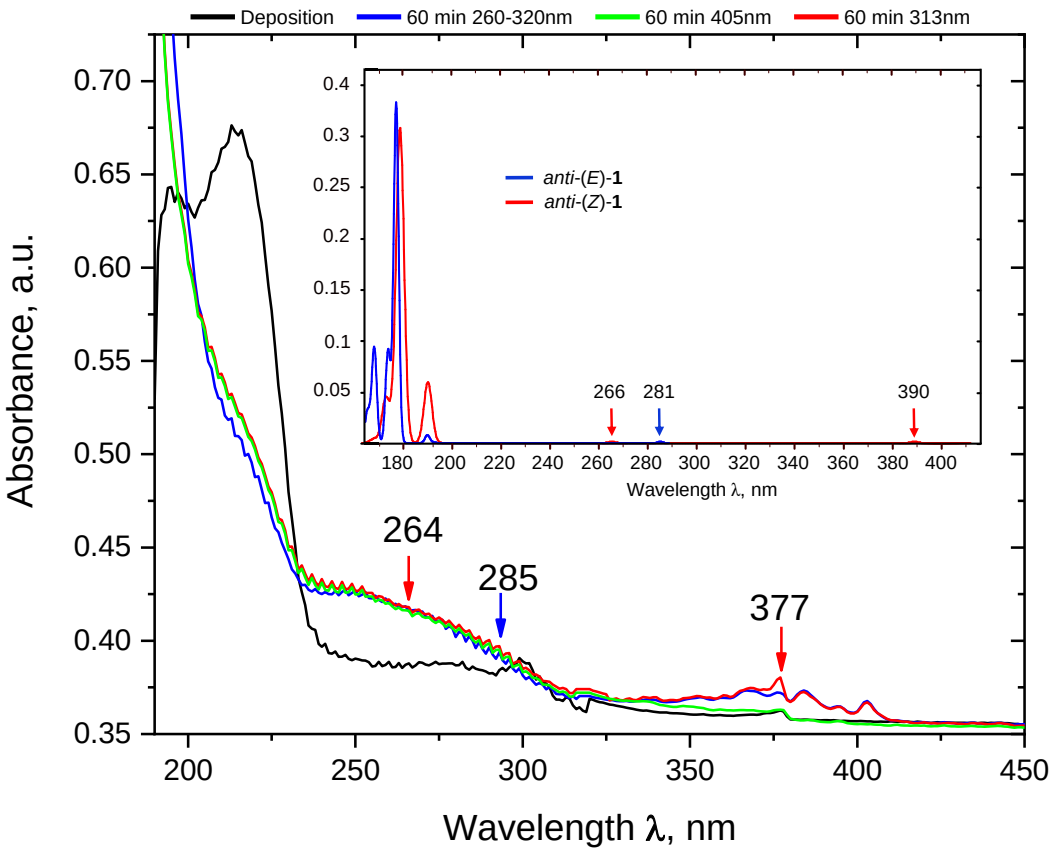

Figure S7. Extension of Figure 2.

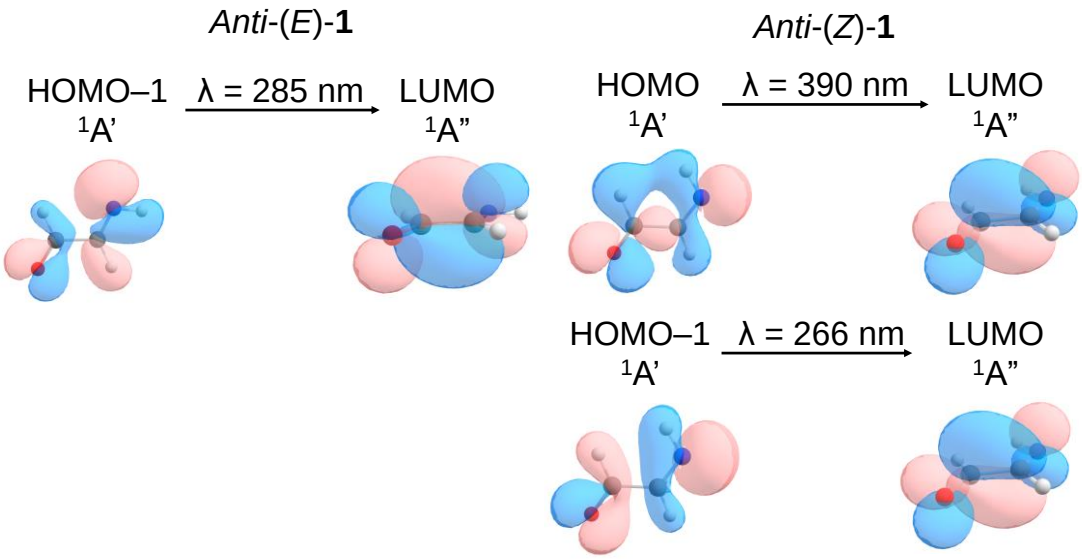

Figure S8. Natural bond orbitals (NBOs) for the electronic transitions of *anti*-(*E*)-**1** and *anti*-(*Z*)-**1** calculated at B3LYP/6-311++G(2d,2p) level of theory. HOMO=highest occupied molecular orbital; LUMO=lowest unoccupied molecular orbital.

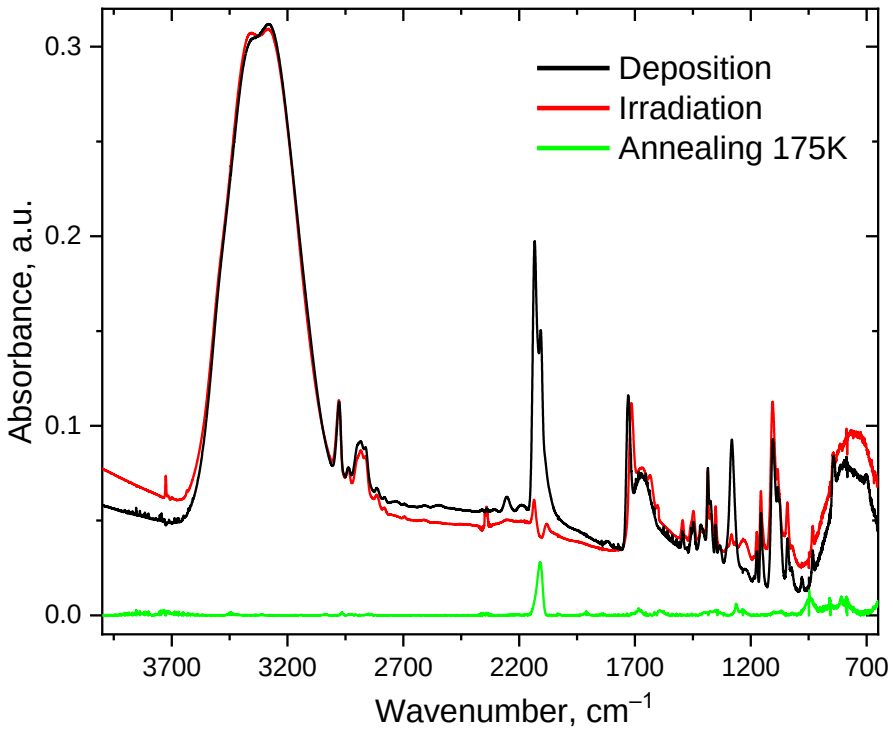

Figure S9. FT-IR spectrum of deposited (black), UV irradiated (red) and annealed to 175 K (green) 2-azidoacetaldehyde (**6**) in water matrix at 3K.

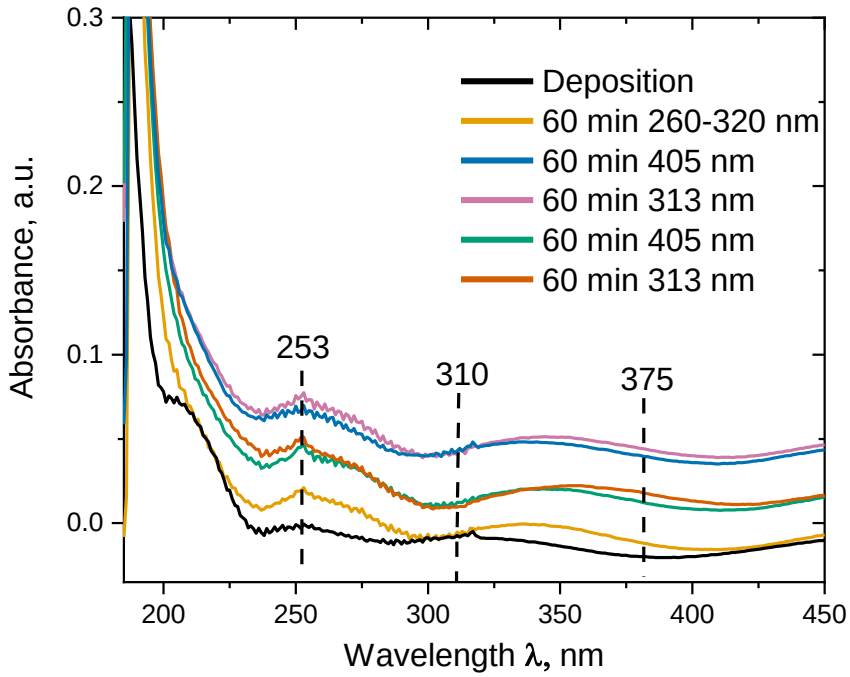

Figure S10. UV/Vis spectra of deposited and photolyzed 2-azidoacetaldehyde (**6**) and conformational interconversion of 2-iminoacetaldehyde conformers (**1**) induced by UV and blue light irradiation in LDA water ice at 3 K.

IR Spectroscopic Data

Table S1. Comparison of experimental vibrational frequencies of *anti*-(*E*)-**1** isolated in an argon matrix at 3 K and computed vibrational frequencies at the CCSD(T)/cc-pVTZ level of theory (unscaled).

Mode	Sym.	$\tilde{\nu}_{harm.}$ / cm^{-1}	$I_{calc.}$ / km mol^{-1}	$\tilde{\nu}_{exp.}$ / cm^{-1}	$I_{rel.}$
3	A’	579.5	1.5	-	-
4	A”	705.4	61.2	691.9	m
5	A”	1035.3	3.7	1018.4	w
6	A’	1038.3	25.1	1011.9	m
7	A”	1122.0	6.3	1086.7 1091.0	w
8	A’	1226.5	35.8	1205.0	m
9	A’	1370.4	11.8	1333.4 1338.5	w
10	A’	1404.5	25.6	1369.4 1378.1	w
11	A’	1662.1	15.1	Overlaps	m
12	A’	1770.9	92.1	1723.9 1726.4	s
13	A’	2982.3	54.7	2853.4	m
14	A’	3092.5	21.7	-	
15	A’	3459.7	1.2	3475.4 tentative	w

rel. experimental intensities (w = weak, m = middle, s = strong)

Table S2. Comparison of experimental vibrational frequencies of *anti*-(*Z*)-**1** isolated in an argon matrix at 3 K and computed vibrational frequencies at the CCSD(T)/cc-pVTZ level of theory (unscaled).

Mode	Sym.	$\tilde{\nu}_{harm.}$ / cm^{-1}	$I_{calc.}$ / km mol^{-1}	$\tilde{\nu}_{exp.}$ / cm^{-1}	$I_{rel.}$
3	A’	568.6	2.4	-	-
4	A”	717.2	9.4	-	m
5	A”	1023.5	0.3	-	m
6	A’	1060.9	56.4	1032.9 1042.8	w
7	A”	1139.3	60.0	1100.9 1107.9	w
8	A’	1236.6	23.9	1210.8	m
9	A’	1392.3	14.4	1353.0	w
10	A’	1404.2	18.0	1362.2	w
11	A’	1655.6	10.9	Overlaps	m
12	A’	1773.0	101.7	1731.3 1735.2	s
13	A’	2909.4	80.0	2812.1	w
14	A’	3148.9	8.8	-	
15	A’	3383.8	2.3	-	w

rel. experimental intensities (w = weak, m = middle, s = strong)

Table S3. Comparison of experimental vibrational frequencies of *anti*-(*E*)-**1**-d_3 isolated in an argon matrix at 3 K and computed vibrational frequencies at the CCSD(T)/cc-pVTZ level of theory (unscaled).

Mode	Sym.	$\tilde{\nu}_{harm.}$ / cm^{-1}	$I_{calc.}$ / km mol^{-1}	$\tilde{\nu}_{exp.}$ / cm^{-1}	$I_{rel.}$
3	A”	529.3	27.3	519.7	m
4	A’	560.8	1.7	-	-
5	A’	816.8	22.9	801.2	m
6	A”	851.8	8.8	831.4	W
7	A”	902.5	0.7	-	-
8	A’	952.6	4.5	939.8	w
9	A’	1055.3	10.2	1038.3 1036.2	w
10	A’	1216.4	18.7	1190.2	m
11	A’	1624.9	16.2	-	m
12	A’	1750.4	92.0	1701.7	s
13	A’	2206.7	45.7	2144.1	m
14	A’	2289.2	14.0	2230.7	w
15	A’	2533.9	1.9	2443.4	w

rel. experimental intensities (w = weak, m = middle, s = strong)

Table S4. Comparison of experimental vibrational frequencies of *anti*-(*Z*)-**1**- d_3 isolated in an argon matrix at 3 K and computed vibrational frequencies at the CCSD(T)/cc-pVTZ level of theory (unscaled).

Mode	Sym.	$\tilde{\nu}_{harm.}$ / cm^{-1}	$I_{calc.}$ / km mol^{-1}	$\tilde{\nu}_{exp.}$ / cm^{-1}	$I_{rel.}$
3	A’	538.8	4.3	-	-
4	A”	568.2	10.8	556.3	w
5	A”	831.9	29.6	813.0	m
6	A’	876.8	40.1	856.5	m
7	A”	894.7	0.4	875.4	w
8	A’	958.7	2.9	944.7	w
9	A’	1069.5	18.0	1044.9 1048.6	w
10	A’	1173.7	1.6	-	-
11	A’	1629.7	11.1	-	m
12	A’	1756.1	97.3	1716.4	m
13	A’	2150.6	62.6	*	m
14	A’	2331.4	7.0	-	-
15	A’	2474.6	0.4	2382.7	w

rel. experimental intensities (w = weak, m = middle, s = strong); *-band overlaps with 2-azidoacetaldehyde-d_3

Table S5.Absorption maxima for the products of 2-azidoacetaldehyde and 2-azidoacetaldehyde-d_3 HVFP in argon matrix at 3 K.

2-azidoacetaldehyde		2-azidoacetaldehyde-d_3	
Name	$\tilde{\nu}_{exp.}$ / cm^{-1}	Name	$\tilde{\nu}_{exp.}$ / cm^{-1}
CO[23]	2138.2	CO[23]	2138.2
HCN[24]	3303.9 721.9	DCN[25]	2626.1 1925.0 575.6
CH_2NH[26]	3035.0 2923.6 1639.7 1346.6 1123.6 1059.3 1064.0	CD_2ND[27]	2141.1 1575.4 1088.1 769.9 820.5
		CD_2O[28]	2091.2 2087.4 986.9
CH_2O[28]	2994.9 2864.2 2789.9 1741.6 1498.9 1168.8	CD_3CN[29]	2268.1 1032.1 849.2
		CD_3NC[29]	2258.9 2159.0
CH_3CN[24]	2258.1 1444.8	CD_2CN•[29]	908.6 543.8
CH_3NC[24]	2159.0 938.2	CD_2NC•[29]	1981.9 850.7
CH_2CN•[24]	1429.2 1025.0 666.1		
CH_2NC•[24]	1068.2 588.1		

UV/Vis Spectroscopic Data

Table S6. TD-DFT B3LYP/6-311++G(2d,2p) computed vertical excitation energies of *anti*-(*E*)-**1** and comparison with the recorded UV/Vis photolysis spectrum.

Excitation energy, λ/nm	Oscillator strength (*f*)	$\lambda_{exp.}$/nm	Transition
281.4	0.0011	285	HOMO–1 – LUMO
192.0	0.0005	Out of range	HOMO – LUMO+2
189.3	0.0068	Out of range	HOMO–1 – LUMO+1 HOMO – LUMO+1

Table S7. TD-DFT B3LYP/6-311++G(2d,2p) computed vertical excitation energies of *anti*-(*Z*)-**1** and comparison with the recorded UV/Vis photolysis spectrum.

Excitation energy, λ/nm	Oscillator strength (*f*)	$\lambda_{exp.}$/nm	Transition
390.0	0.0010	377	HOMO – LUMO
266.1	0.0016	264 (tentative)	HOMO–1 – LUMO HOMO – LUMO+2
190.7	0.0586	Out of range	HOMO – LUMO+1 HOMO–2 – LUMO

NMR Spectra

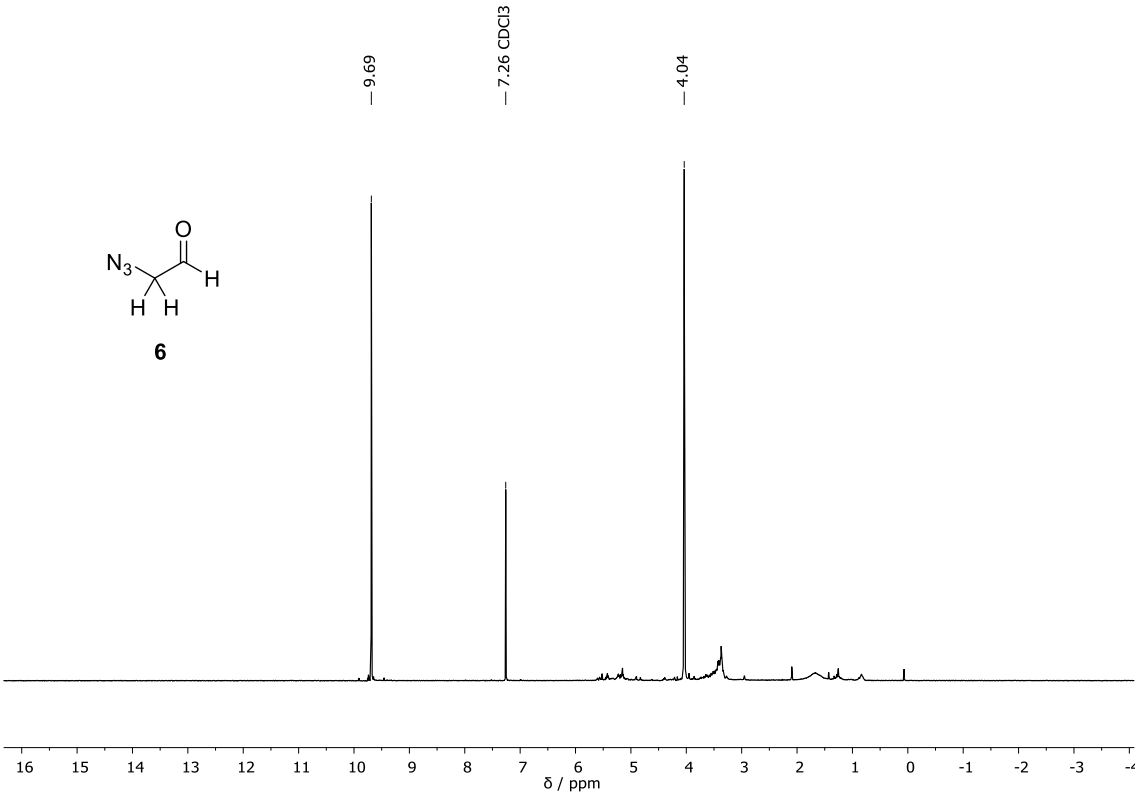

Figure S10. ^{1}H NMR (400 MHz, $CDCl_3$) spectrum of 2-azidoacetaldehyde (**6**).

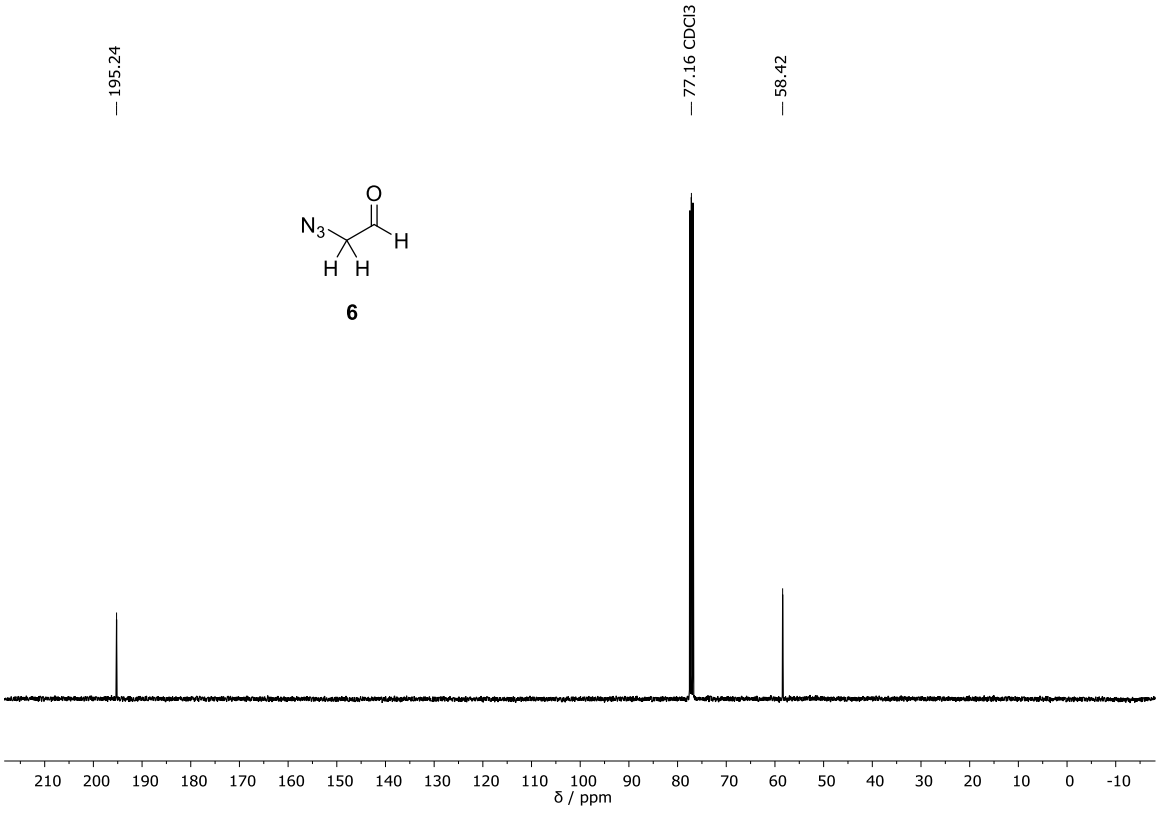

Figure S11. $^{13}C\{^{1}H\}$ NMR (101 MHz, $CDCl_3$) spectrum of 2-azidoacetaldehyde (**6**).

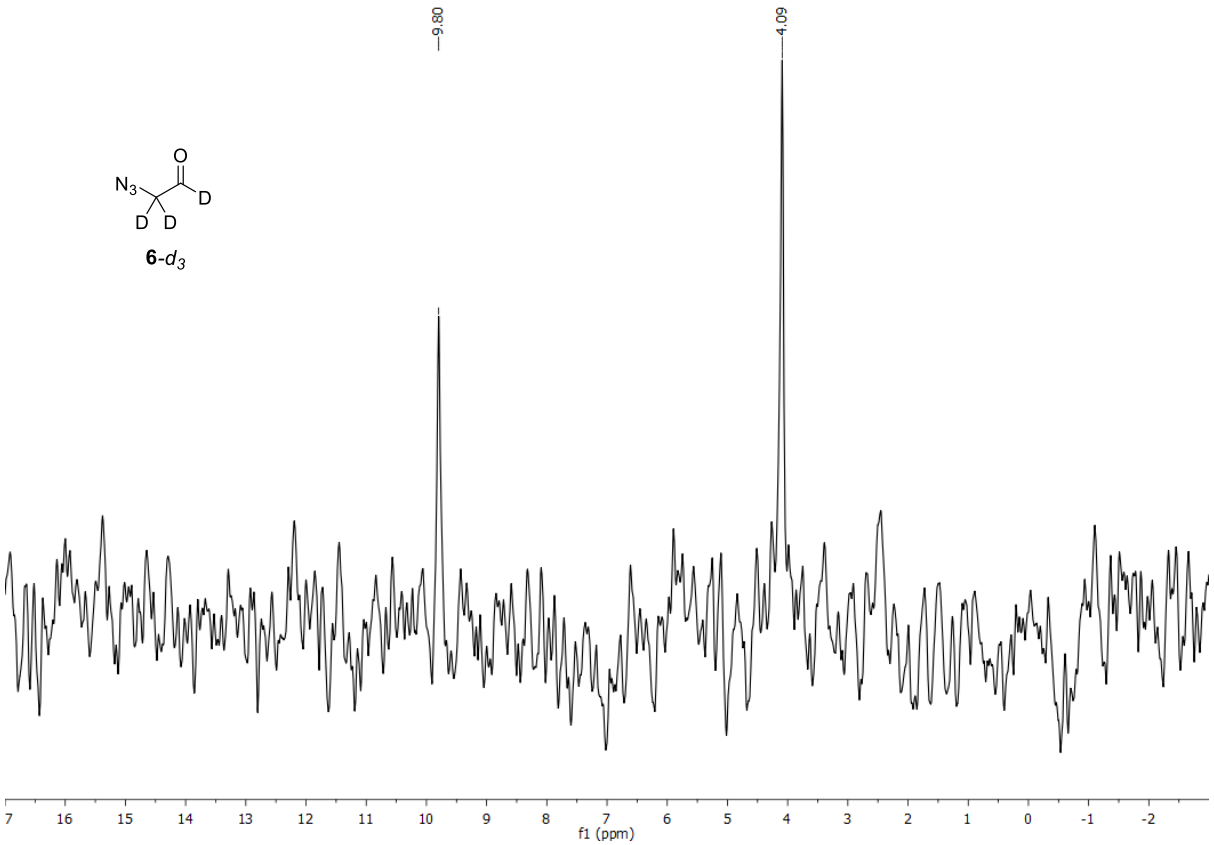

Figure S12. ^{2}D NMR (61 MHz, $CHCl_3$) spectrum of 2-azidoacetaldehyde-d_3 (**6**-d_3).

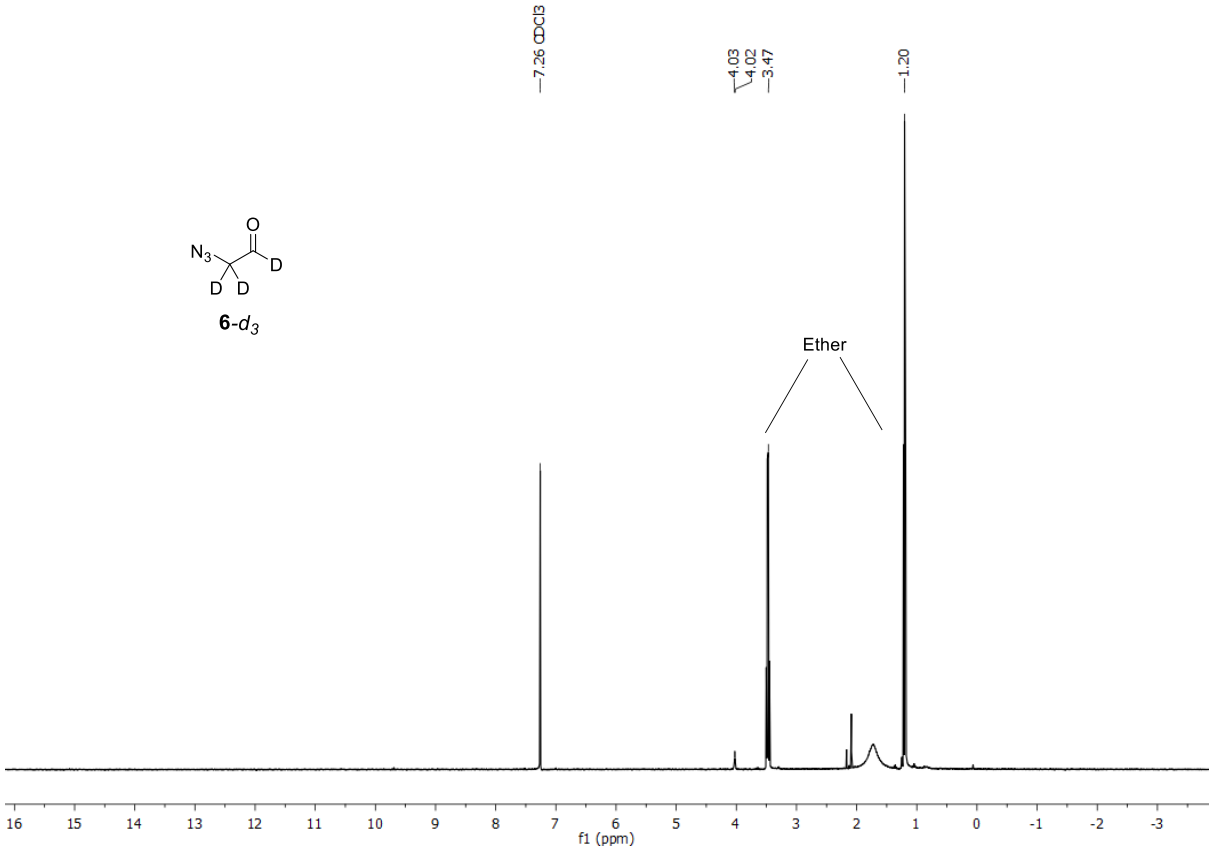

Figure S13. ^{1}H NMR (400 MHz, $CDCl_3$) spectrum of 2-azidoacetaldehyde-d_3 (**6**-d_3).

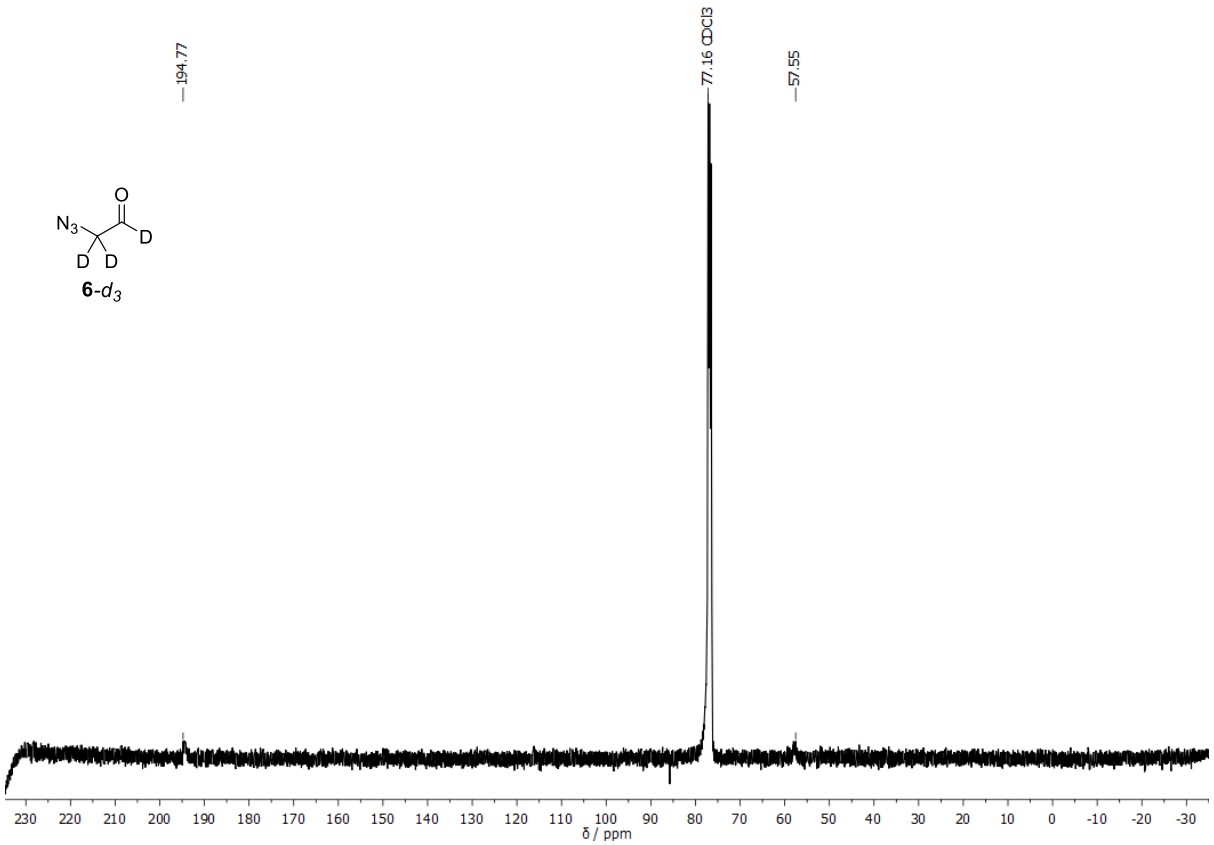

Figure S14. $^{13}C\{^{1}H\}$ NMR (101 MHz, $CDCl_3$) spectrum of 2-azidoacetaldehyde-d_3 (**6**-d_3). Note that the spectrum was taken on a different day than the ^{1}H spectrum depicted in Figure S13 and diethyl ether was completely removed from the sample.

Potential Energy Surfaces and Electronic Energies for Selected Structures

Table S8. B3LYP/6-311++G(2d,2p) optimized structures, electronic energies (in Hartree), zero-point vibrational energies (ZPVEs in Hartree), CCSD(T)/CBS energies (in Hartree) and relative energies of all structures depicted in Figure.

Compound	E	ZPVE	CCSD(T)/CBS	ΔE(B3LYP) / kcal mol^{-1}	ΔE(CCSD(T)) / kcal mol^{-1}
2-azidoacetaldehyde (**6**)	–317.510906	0.059552	–317.064180	51.5	55.8
anti-(*Z*)-**1**	–208.023342	0.049851	–207.725264	1.3	1.2
anti-(*E*)-**1**	–208.025498	0.049950	–207.727342	0.0	0.0
syn-(*Z*)-**1**	–208.021803	0.050020	–207.724360	2.4	1.9
syn-(*E*)-**1**	–208.015868	0.049407	–207.718030	5.7	5.5
TS1	–207.816785	0.042998	–207.595531	126.6	78.4
TS2	–207.894596	0.042812	–207.589728	77.7	81.9
TS3	–207.930803	0.047013	–207.628314	57.6	60.3
TS4	–207.982150	0.047002	–207.681429	25.4	27.0
TS5	–208.01334	0.049043	–207.715566	7.1	6.8
TS6	–208.013415	0.04894	–207.715866	6.9	6.6
TS7	–207.975735	0.046713	–207.675236	29.2	31
HNC (+**7**)	–93.434009	0.015327	–93.292604	24.0	23.4
HCN (+**7**)	–93.456798	0.016259	–93.316210	10.3	9.2
CH_2O (**7**)	–114.545181	0.026524	–114.389345		
CO (+**2**)	–113.352012	0.005037	–113.206210	1.1	–1.2
CH_2NH (**2**)	–94.666690	0.039854	–94.517936		
N_2	–109.563481	0.005547	–109.421709		

Table S9. B3LYP/6-311++G(2d,2p) optimized conformers and relative energies of 2-azidoacetaldehyde (**6**) based on a conformational search using CREST.

Conformer	E	ZPVE	CCSD(T)/CBS	ΔE(B3LYP) / kcal mol^{-1}	ΔE(CCSD(T)) / kcal mol^{-1}
1	–317.510906	0.059552	–317.064180	0.0	0.0
2	–317.509941	0.059274	–317.062676	0.4	0.8
3	–317.510661	0.059035	–317.063227	–0.2	0.3
4	–317.508219	0.059215	–317.060768	1.5	1.9

References

1 E. Whittle, D. A. Dows and G. C. Pimentel, *J. Chem. Phys.*, **1954**, 22, 1943.
2 Gaussian 16, Revision C.01, M. J. Frisch, G. W. Trucks, H. B. Schlegel, G. E. Scuseria, M. A. Robb, J. R. Cheeseman, G. Scalmani, V. Barone, G. A. Petersson, H. Nakatsuji, X. Li, M. Caricato, A. V. Marenich, J. Bloino, B. G. Janesko, R. Gomperts, B. Mennucci, H. P. Hratchian, J. V. Ortiz, A. F. Izmaylov, J. L. Sonnenberg, D. Williams-Young, F. Ding, F. Lipparini, F. Egidi, J. Goings, B. Peng, A. Petrone, T. Henderson, D. Ranasinghe, V. G. Zakrzewski, J. Gao, N. Rega, G. Zheng, W. Liang, M. Hada, M. Ehara, K. Toyota, R. Fukuda, J. Hasegawa, M. Ishida, T. Nakajima, Y. Honda, O. Kitao, H. Nakai, T. Vreven, K. Throssell, J. A. Montgomery, Jr., J. E. Peralta, F. Ogliaro, M. J. Bearpark, J. J. Heyd, E. N. Brothers, K. N. Kudin, V. N. Staroverov, T. A. Keith, R. Kobayashi, J. Normand, K. Raghavachari, A. P. Rendell, J. C. Burant, S. S. Iyengar, J. Tomasi, M. Cossi, J. M. Millam, M. Klene, C. Adamo, R. Cammi, J. W. Ochterski, R. L. Martin, K. Morokuma, O. Farkas, J. B. Foresman, and D. J. Fox, Gaussian, Inc., Wallingford CT, **2016.**
3 A. D. Becke, *J. Chem. Phys.*, **1993**, 98, 5648–5652.
4 C. Lee, W. Yang and R. G. Parr, *Phys. Rev. B*, **1988**, 37, 785–789.
5 A. D. Becke, *Phys. Rev. A*, **1988**, 38, 3098–3100.
6 R. Krishnan, J. S. Binkley, R. Seeger and J. A. Pople, *J. Chem. Phys.*, **1980**, 72, 650–654.
7 T. Clark, J. Chandrasekhar, G. W. Spitznagel and P. V. R. Schleyer, *J. Comput. Chem.*, **1983**, 4, 294–301.
8 E. Runge and E. K. U. Gross, *Phys. Rev. Lett.*, **1984**, 52, 1000.
9 R. Bauernschmitt and R. Ahlrichs, *Chem. Phys. Lett.*, **1996**, 256, 454–464.
10 R. E. Stratmann, G. E. Scuseria and M. J. Frisch, *J. Chem. Phys.*, **1998**, 109, 8218–8224.
11 T. H. Dunning, *J. Chem. Phys.*, **1989**, 90, 1007–1023.
12 R. A. Kendall, T. H. J. Dunning and R. J. Harrison, *J. Chem. Phys.*, **1992**, 96, 6796–6806.
13 A. K. Wilson, T. Van Mourik and T. H. Dunning, *J. Mol. Struct. THEOCHEM*, **1996**, 388, 339–349.
14 T. Helgaker, W. Klopper, H. Koch and J. Noga, *J. Chem. Phys.*, **1997**, 106, 9639–9646.
15 S. Zhong, E. C. Barnes and G. A. Petersson, *J. Chem. Phys.*, **2008**, 129, 184116.
16 A. Halkier, T. Helgaker, P. Jørgensen, W. Klopper, H. Koch, J. Olsen and A. K. Wilson, *Chem. Phys. Lett.*, **1998**, 286, 243–252.
17 F. Neese, *Wiley Interdiscip. Rev. Comput. Mol. Sci.*, **2018**, 8, 4–9.
18 C. Bannwarth, S. Ehlert and S. Grimme, *J. Chem. Theory Comput.*, **2019**, 15, 1652–1671.
19 C. Bannwarth, E. Caldeweyher, S. Ehlert, A. Hansen, P. Pracht, J. Seibert, S. Spicher and S. Grimme, *Wiley Interdiscip. Rev. Comput. Mol. Sci.*, **2021**, 11, 1–49.
20 P. Pracht, F. Bohle and S. Grimme, *Phys. Chem. Chem. Phys.*, **2020**, 22, 7169–7192.
21 Chemcraft - graphical software for visualization of quantum chemistry computations. Version 1.8, build 654. https://www.chemcraftprog.com.
22 K. Ii, S. Ichikawa, B. Al-Dabbagh, A. Bouhss and A. Matsuda, *J. Med. Chem.*, **2010**, 53, 3793–3813.
23 H. Dubost, *Chem. Phys.*, **1976**, 12, 139–151.
24 S. V Kameneva, A. D. Volosatova and V. I. Feldman, *Radiat. Phys. Chem.*, **2017**, 141, 363–368.
25 C. M. King and E. R. Nixon, *J. Chem. Phys.*, **1968**, 48, 1685–1695.
26 M. E. Jacox and D. E. Milligan, *J. Mol. Spectrosc.*, **1975**, 56, 333–356.
27 D. E. Milligan, *J. Chem. Phys.*, **1961**, 1491, 1491–1497.
28 C. Lugez, A. Schriver, R. Levant and L. Schriver-Mazzuoli, *Chem. Phys.*, **1994**, 181, 129–146.
29 A. D. Volosatova, S. V Kameneva and V. I. Feldman, *Phys. Chem. Chem. Phys*, **2019**, 13014–13021.